

The Unsteady Near-Wake of a Simplified Passenger Car

G. Vino¹, S. Watkins¹, P. Mousley², J. Watmuff¹ and S. Prasad¹

¹ School of Aerospace, Mechanical and Manufacturing Engineering
RMIT, Melbourne, Australia

²Turbulent Flow Instrumentation Pty Ltd, Tallangatta, Australia

Abstract

The time-averaged and time-dependant nature of the wake of a simplified passenger vehicle (Ahmed model) has been investigated experimentally. Time-averaged results of the far-wake showed good agreement to previously published work, although the near-wake structure was found to be somewhat different, complementing findings made through flow visualisation. Time-dependant analysis revealed that the shedding behind the model is analogous to vortex shedding behind simple bluff bodies, with most of the fluctuations confined to the axial and vertical directions. In addition, the shedding characteristics on the slant showed very similar behaviour to the vertical base, indicating strong turbulent mixing between the two regions, emphasizing time-averaged findings and complementing the proposed flow topology.

Introduction

There exists a large database of information directed towards understanding flow structures in the wake of simplified passenger vehicle geometries. Until recently, the bulk of literature has only been successful in elucidating regions in the wake where the flow direction is dominantly in the streamwise sense. In addition, much of this work has been limited to time-averaged behaviour, due to the complexity associated with time-varying flows that exhibit significant flow angles, and sometime complete reversals.

The purpose of this research is to further the understanding of flow in the near-wake of a well-known simplified passenger vehicle geometry.

The use of simplified forms of passenger vehicles has proven extremely useful in terms of understanding the fundamental flow characteristics associated with more complex passenger cars [5]. Although many types of simplified passenger vehicle geometries have been investigated, one of the most popular has been the Ahmed model, after [1]. From flow visualisation and time-averaged measurements, the hypothesised flow patterns of Ahmed et al are summarized in Figure 1. It is important to note that some of the time-averaged results presented indicate that certain complex flow regions (i.e. large flow angles including reversals) were not successfully captured during sampling, although this was not discussed in detail.

The size and strength of the C-pillar vortices were found to be very dependant on the base slant angle. As the base slant angle reached 30 degrees from the horizontal, the separated bubble on the slanted edge grows in size forming a dominant low-pressure horseshoe vortex on the backlight. This low-pressure region then draws in and strengthens the C-pillar vortices. Overall, the base pressure is significantly reduced, resulting in a significant rise in drag. Beyond a slant angle of 30 degrees, the separated flow is no longer able to reattach down the slanted edge, thus reducing the strength of the C-pillar vortices. Hence, at slant angles above 30 degrees the flow pattern is accompanied by a significant rise in base pressure and therefore reduction in drag. The "critical" 30-degree high-drag backlight configuration was used in this investigation.

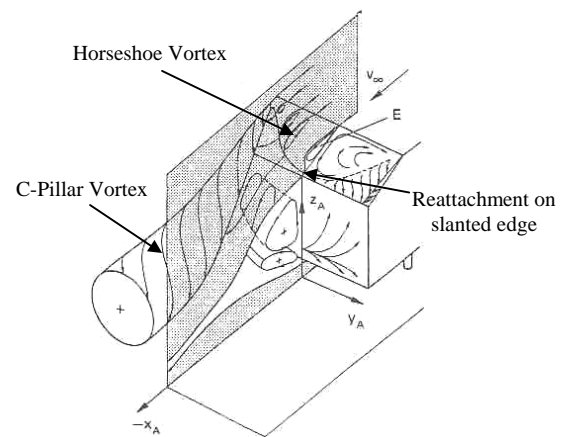


Figure 1. Proposed high-drag vortex system for the Ahmed model geometry [1].

This paper will further elucidate the complex behaviour in this near-wake region through a detailed experimental investigation into the time averaged and unsteady flow characteristics.

Experimental Arrangement

A 1/4 scale Ahmed model geometry was used in this investigation, with the rear slant angle held constant at 30 degrees. All tests in this investigation were conducted in the RMIT Industrial Wind Tunnel. The wind tunnel is a closed-jet and fixed-ground type, and is able to generate flow speeds of up to 43 m/s, with a longitudinal turbulence intensity of 1.5%. The wind-tunnel blockage ratio was equal to 1.9%, based on maximum projected frontal area of the Ahmed model, which was deemed suitable in that relevant flow structures would not be significantly affected by the presence of the wind tunnel walls. No corrections were made for blockage.

Time-averaged and time-varying surface pressure measurements were measured with a Dynamic Pressure Measurement System (DPMS), supplied by Turbulent Flow Instrumentation Pty Ltd. Tests were conducted at a range of speeds between 20 and 35 m/s. Silicon tubes of 0.8 mm diameter were inserted at each surface pressure tap and connected to the DPMS. As described in [5] and [2], the oscillatory pressures through these tubes undergo an amplitude variation and phase lag that is frequency dependant. Therefore, the pressure signals measured by the transducers were linearised to correct for the amplitude and phase distortion. The correction technique used is based on a Fourier transform technique (see [3]) and consists of obtaining the Fourier transform of the measured signal at the transducer, dividing this by a tubing transfer function (that relates the dynamic pressure at the transducer to that at the point of measurement), and transforming the result back to the time domain via an Inverse Fourier transform.

In order to obtain a more complete representation of the flow field, off-body flow measurements were taken at three downstream transverse planes in the wake of the model. Single

point flow measurements were conducted at a wind tunnel speed of 35 m/s using a 13-hole, high frequency response pressure probe. This pressure probe, known as the ECA (Extended Cone of Acceptance) Probe, was also supplied by Turbulent Flow Instrumentation. It is of the multi-hole type and has a flow acceptance cone of about $\pm 135^\circ$, resolving all three components of velocity and local static pressure up to frequencies of about 1 KHz. For more information on the design, validity, steady state and dynamic calibration of the probe, refer to [12].

Results

Time-Averaged Results

Figure 2 shows the off-body flow patterns at the rear of the model through smoke injection. In the top figure the smoke was injected at the end of the roof centerline, while the smoke patterns shown in lower figure originated at the top of the C-pillar as shown. The wake pattern shows excellent agreement with [10], in that the flow over the backlight shows a large separation bubble over the entire centerline, consequently aiding the generation of a strong trailing vortex from the C-pillar, which is very well defined. It is important to note however that unlike the proposed flow pattern of [1], the flow along the centreline does not fully reattach before leaving the base, but forms part of the wake behind.

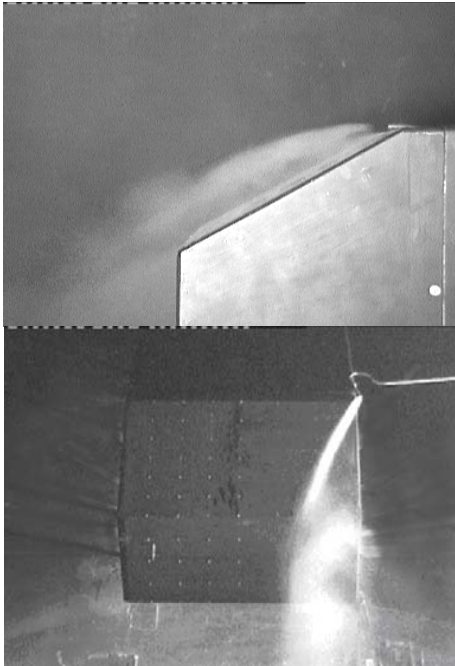


Figure 2. Off-body smoke flow patterns at rear end of the model.

Figure 3 shows the corresponding surface skin friction patterns on the backlight and vertical base. It is evident that the flow from the roof separates at the top of the backlight, which is consistent with smoke flow patterns. Just inboard of the C-pillars, there exists a separation line extending through the entire length of the backlight. This line makes an angle of approximately 7 degrees relative to the C-pillar, comparing well to results obtained by [10] and [1]. It has been widely accepted that this separation line is a result of the C-pillar vortex separating as it spirals along the backlight.

Further inboard there is a large separated region that extends to the base of the backlight. Many authors have also revealed the existence of this large separated region, which is bordered by the trailing vortex impingement lines. These impingement lines also agree with smoke patterns shown in Figure 2. Within this region exist significant levels of reverse flow making a radiating pattern originating from main stable foci located just below the top

corners of the backlight. The presence of these foci corresponds to the work of [11]. In addition, unlike [1] whereby this reverse flow region was fully enclosed and assumed an arch shaped horseshoe vortex (see Figure 1), this region takes on a 'D - like' shape, with a central tail at its base. This central tail, which is relatively thin, does not show any sign of reattachment but instead exhibits flow reversals right up until the rear of the model. A similar shaped detached flow region was also found by [10]. Thus, it is envisaged that the separated flow over the slant reattaches along the vortex impingement lines, but not in the small region between.



Figure 3. Rear end surface skin friction patterns.

On the vertical base, there exists a well-defined line that makes the shape of an arch. The patterns suggest that the flow originates at the periphery of this arch and radiates towards the top and sides of the base. Within the arch, patterns made during model preparation (i.e. applying surface oil solution) are significant, indicating low levels of energy within this region. This suggests that the flow just off the surface of the vertical base is characterised by a dominant arch-shaped recirculation bubble. It is envisaged that a counter-rotating vortex is created below, which is fed below by the flow coming from the underbody and above by this large arch vortex, although this is not discernable from Figure 3.

Figure 4 shows the mean velocity vectors measured with the ECA probe along the plane of symmetry and Figure 5 shows the corresponding calculated streamline pattern. Thus far, this complex near-wake flow region has proven difficult to capture due to the limitations associated with hot-wire and pressure probes measuring flow reversals, however, flow structures within this region were successfully captured with the 13-hole probe.

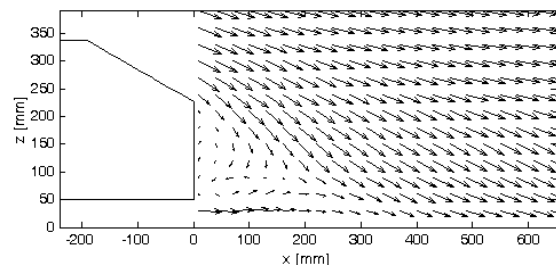


Figure 4. Velocity vectors measured along the symmetry plane in wake of model.

Through the use of PIV, [7] were also able to capture flows in the near-wake, although the data published and conclusions drawn were somewhat limited to far-wake characteristics.

Immediately behind the vertical base, a well-defined separation at the top and bottom of the vertical base is apparent, enclosing a clear recirculatory flow region. Two recirculatory bubbles are observed, one above the other, and in opposing directions. The higher bubble covers the upper region of the

vertical base, while the lower bubble, which rotates in the opposite direction, does not appear to interact with the surface. This finding agrees with skin friction patterns of Figure 3, which indicated that a single recirculation bubble interacted with the vertical rear surface.

Towards the upper portion of the separated region it is clear that the circulation zone is drawing fluid from the separated flow above the slanted edge. Thus, the flow over the slanted edge, at least along the centreline, does not reattach on the slant before separating at the base, which emphasises flow patterns in Figure 3. This is in contrast to the flow topology of Ahmed et al [1], which suggests that flow above the central region of the slant is characterised by a large separation bubble that reattaches before separating again at the base. Thus, the closed horseshoe vortex proposed by Ahmed et al is in fact partially open, and mixes with the upper recirculation bubble on the vertical base. As a result, the flow leaving the top of the model assumes much larger angles to the slant.

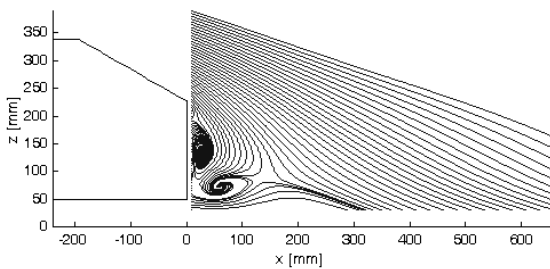


Figure 5. Streamlines along the symmetry plane in wake of model.

This finding also agrees with the work of [11], which shows that the horseshoe vortex on the slant was not closed but mixed with the flow in the wake. It is important to note that the model used by [11] had a slant angle of just 25 degrees, which would only act to promote reattachment. Thus, this new proposed flow topology is not limited to slant angles very close to and above the critical geometry (i.e. 30 degrees rear slant angle).

Unsteady Results

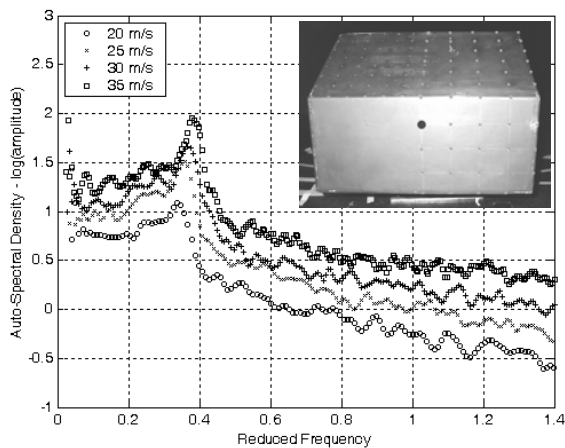


Figure 6. Auto-spectral Density function of a selected surface pressure tap on the rear of the model.

Although only shown here for a single location (see Figure 6), spectral analysis of time-signals of various surface pressure taps on the rear slant and vertical base revealed a single dominant shedding frequency of 40 Hz at the highest test Reynolds number, which corresponds to a Strouhal number 0.39 (based on the square root of model frontal area). Some sensitivity of the Strouhal number was also observed within the Reynolds number range tested. Readings from pressure taps on both the vertical

base and slanted edge indicate high energies are also associated with the shedding.

Figure 7 shows the correlation between time signals of surface pressure taps at the top and bottom of the vertical base, corresponding to the two-recirculatory bubbles, one above the other, shown in Figure 1 and Figure 5. Firstly, we see that the phase estimate near the non-dimensional shedding frequency of 0.39 suggests that the shedding is 180 degrees out of phase, implying alternate shedding. Thus, the recirculatory bubbles located behind the vertical base (see Figure 5) are analogous to the well-known von Karman vortex shedding behind bluff bodies, particularly square cylinders, shedding alternately at a Strouhal number of about 0.39. For the test speed range used here, Reynolds numbers (based on square root of frontal area) were between $5.5 \times 10^5 < Re < 7.7 \times 10^5$.

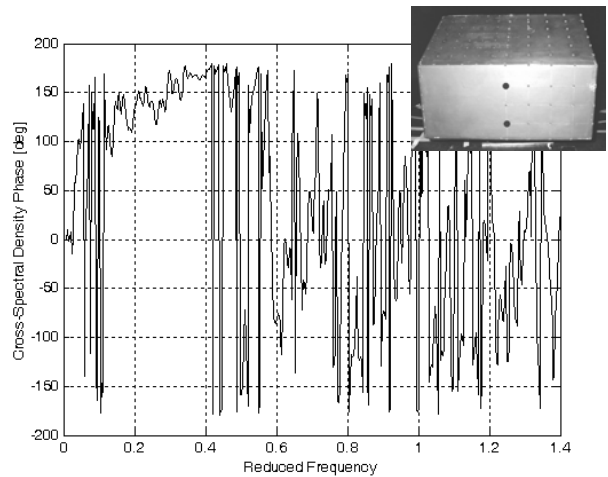


Figure 7. Cross-spectral Phase estimate between selected surface pressure taps on the vertical base.

It is known that at such high Reynolds numbers, circular cylinders exhibit significant losses in periodic flow (see [8]) due the boundary layer undergoing transition to turbulence, creating a smaller wake, and accompanied by diminishing shedding characteristics. However, square cylinders tend to exhibit well-defined shedding behaviour up to Reynolds numbers well beyond those investigated here due to the separation locations being fixed irrespective of Reynolds number, which result in well-defined separated shear layers at opposite sides of the wake.

Time-averaged results suggest that the flow over the slant mixes with the upper recirculation bubble behind the vertical base. Figure 8 shows the correlation of shedding characteristics between pressure taps on the slant and upper region of the vertical base. At a reduced frequency of 0.39, the two regions correlate close to 0 degrees, suggesting that they are in phase. Thus, the fluctuations on the slanted edge shed simultaneously with the upper separation bubble on the vertical base. This result emphasizes that the detached flow region on the slant and recirculation bubble on the vertical base are in fact a single large separated flow region.

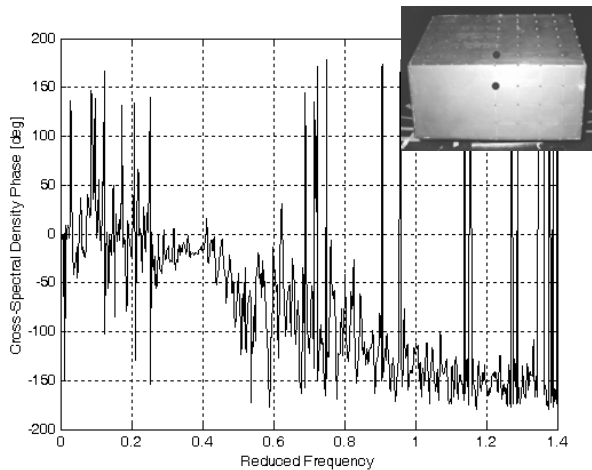


Figure 8. Cross-spectral Phase estimate between surface pressure taps on the slant and vertical base.

Proposed Flow Topology

Figure 9 highlights the important time-averaged flow features found from this investigation, with surface patterns drawn as limiting streamlines (i.e. lines of surface shear stress) on the right hand side of the model, and off-body flows on the left.

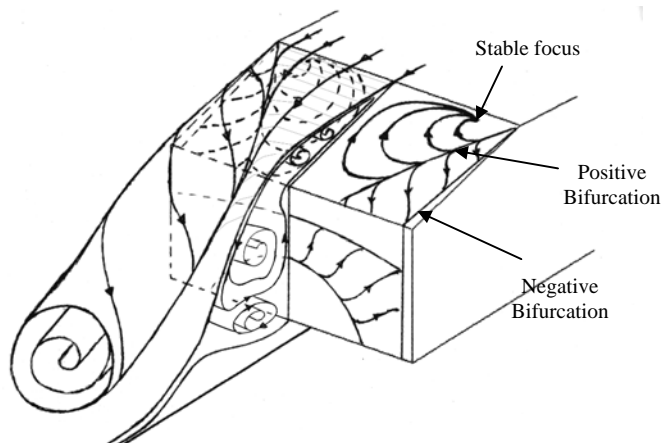


Figure 9. Proposed topological flow structure of the Ahmed model with critical geometry.

Clearly, the impingement of the trailing vortex along the C-pillar is shown. This impingement can be considered as a classic example of a positive bifurcation in terms of the 'critical point theory' described in [7] and [3]. Here, a streamline from the oncoming stream surface (i.e. the trailing vortex surface) bifurcates into two at the line. On one side of this positive bifurcation, the flow tends toward a stable focus in a spiralling path, as it interacts with the flow reversals inside the detached flow region on the slant. On the other side, the path taken by the vortex as it interacts with the surface is shown. Note that the vortex separates at approximately 7 degrees to the C-pillar. Although not found in results of this study, possibly due to limited resolution of flow maps, [10] showed that a smaller, counter rotating, vortex existed above the small region between the line and C-pillar. As such, this 7-degree separation line can be viewed as a negative bifurcation, in which two streamlines appear to combine into one.

On the vertical base, the limiting streamlines indicate the path of the upper separation bubble, which causes significant levels of upwash on the surface. Note the horseshoe shape made by the bubble as it extends to the sides of the model. No

hypothesis is made for the regions above and below this bubble since results failed to reveal any definite path.

Off the body, the combination of the detached flow over the backlight and recirculation bubble on the vertical base is shown. It is important to note that although the detached flow region on the slanted edge only fails to reattach in the small region between the trailing vortices, it does reattach along the positive bifurcation lines. Also, it was found that this region was highly unsteady, so the time-averaged flow topology should only serve as an approximate representation. Finally, the dominant trailing vortex generated at the C-pillar is also shown, with its path illustrating that the vortex core tends to move downward as it flows downstream.

Concluding Remarks

The complex nature of the near- and far-wake of the Ahmed model geometry has been investigated. Surface friction patterns and time-averaged results revealed that the separated flow region over the slanted edge does not fully reattach further down the slant, but instead mixes with the large separated region behind the vertical base. The two regions consequently exhibit similar time-dependant behaviour.

Spectral characteristics of surface pressure signals also revealed that the recirculation bubbles found behind the vertical base could be seen as analogous to longitudinal vortices in a von Karman vortex street.

References

- [1] Ahmed, S.R., Ramm, G. & Faltin, G., Some Salient Features of the Time-Averaged Ground Vehicle Wake, *Society of Automotive Engineers*, 1984, 840300.
- [2] Bergh, H. & Tidjeman, H., Theoretical and Experimental Results for the Dynamic Response of Pressure Measuring Systems, *National Aero And Aeronautical Research Institute*, 1965, NLR-TR F.238.
- [3] Hooper, J. D. and Musgrove, A. R., Reynolds stress, mean velocity, and dynamic static pressure measurement by a four-hole pressure probe, *Journal of Experimental Thermal and Fluid Science*, **15**, 1997, 375-383.
- [4] Hornung, H. & Perry, A. E., Some Aspects of Three-Dimensional Separation, Part 1: Stream surface Bifurcations, *Z. Flugwiss. Weltraumforsch* **8**, 1984, 77-87.
- [5] Iberall, A. S., Attenuation of Oscillatory Pressures in Instrument Lines, U.S. *Department Of Commerce, National Bureau Of Standards* **45**, 1950, RP2115.
- [6] Le Good, G. & Garry, K. P., On The Use of Reference Models in Automotive Aerodynamics, *Society of Automotive Engineers*, 2004, 04B-25.
- [7] Lienhart, H. & Becker, S., Flow and Turbulence Structure in the Wake of a Simplified Car Model, *Society of Automotive Engineers*, 2003, 2003-01-0656.
- [8] Perry, A. E. & Chong, M. S., A Description of Eddying Motions and Flow Patterns Using Critical-Point Concepts, *Annual Rev. Fluid Mechanics* **19**, 1987, 125-155.
- [9] Roshko, A., Perspectives on Bluff Body Aerodynamics, *Journal Of Wing Engineering And Industrial Aerodynamics* **49**, 1993, 79-100.
- [10] Sims-Williams, D.B., Self-Excited Aerodynamic Unsteadiness Associated with Passenger Cars, PhD Thesis, University Of Durham.
- [11] Spohn, A. & Gillieron, P. 2002 Flow Separations Generated by a Simplified Geometry of an Automotive Vehicle, IUTAM Symp. 2001.
- [12] Vio, G. & Watkins, S. 2004 A Thirteen-Hole Probe for Measurements in Bluff Body Wakes, *Fifth International Colloquium on Bluff Body Aerodynamics and Applications*, Canada, 2004.